

Prediction model based on ¹⁸F-FDG PET/CT radiomic features and clinical factors of EGFR mutations in lung adenocarcinoma

Hong-Yue ZHAO¹, Ye-Xin SU², Lin-Han ZHANG¹, Peng FU^{1,*}

¹Department of Nuclear Medicine, The First Affiliated Hospital of Harbin Medical University, Harbin, Heilongjiang, China; ²Department of Radiology, The First Affiliated Hospital of Harbin Medical University, Harbin, Heilongjiang, China

*Correspondence: fupeng0451@163.com

Received December 22, 2020 / Accepted April 20, 2021

The aim of this study was to build a prediction model for epidermal growth factor receptor (EGFR) mutations in lung adenocarcinoma. A retrospective analysis was performed on 88 patients with lung adenocarcinoma. All patients underwent an ¹⁸F-FDG PET/CT scan and genetic testing of EGFR before the treatment. In the training set, the radiomic features and clinical factors were screened out, and model-1 based on CT radiomic features, model-2 based on PET radiomic features, model-3 based on clinical factors, and model-4 based on radiomic features combined with clinical factors were established, respectively. The performance of the prediction model was assessed by area under the receiver operating characteristic (ROC) curve (AUC). The DeLong test was used to compare the performance of the models to screen out the optimal model, and then built the nomogram of the optimal model. The effect and clinical utility of the nomogram was verified in the validation cohort. In our analysis, model-4 was superior to the other prediction models in identifying EGFR mutations. The AUC was 0.864 (95% CI: 0.777-0.950), with a sensitivity of 0.714 and a specificity of 0.784. The nomogram of model-4 was established. In the validation cohort, the concordance index (C-index) value of the calibration curve of the nomogram model was 0.778 (95%CI: 0.585–0.970), and the nomogram had a good clinical utility. We demonstrated that the model based on ¹⁸F-FDG PET/CT radiomic features combined with clinical factors could predict EGFR mutations in lung adenocarcinoma, which was expected to be an important supplement to molecular diagnosis.

Key words: lung adenocarcinoma, radiomics, epidermal growth factor receptor, positron emission tomography/computed tomography

Lung cancer is the malignant tumor with the highest incidence and mortality worldwide [1, 2]. Lung adenocarcinoma accounts for 40% of all lung cancer cases and is the most common type of pathological pattern of lung cancer [3–5]. Nearly 50% of Asians with adenocarcinoma carries epidermal growth factor receptor (EGFR) mutations [6, 7]. Fortunately, tyrosine kinase inhibitor (TKI) is superior to chemotherapy in progression-free survival and the objective response rate for lung cancer patients with EGFR mutations [8]. However, TKI is less effective in EGFR wild-type lung cancer, and cisplatin-based chemotherapy has a better effect on patients with EGFR wild-type [9, 10]. In clinical practice, the identification of EGFR gene status before treatment is crucial for therapeutic decision-making in lung adenocarcinoma [11]. At present, the diagnosis of EGFR mutations relies on molecular diagnostic of tissues or cells, whereas tumor tissues or cells are usually difficult to obtain, especially in patients who are in poor health or refuse invasive tests,

yet tumor heterogeneity is an inevitable problem in molecular testing [12, 13]. Indeed, liquid biopsy via plasma EGFR mutation tests using cell-free circulating tumor DNA (ctDNA) has been identified currently in Europe as an alternative for EGFR mutation detection when a biopsy of tumor lesions cannot be performed [14], but the detection ability of plasma ctDNA gene mutations is affected by tumor burden. The false-negative rate of patients with a small tumor burden will increase significantly [15]. At the same time, the accumulation of somatic mutations in aging cells will also affect the detection effect of ctDNA [15]. Thus, we need a non-invasive and more convenient method to distinguish between EGFR mutation and EGFR wild-type.

Radiomics is defined as a discipline that extracts high-throughput imaging feature data from medical images, converts the extracted data into a high-dimensional data space that can be mined by automatic or semi-automatic algorithms, and uses statistics or artificial intelligence

technology to analyze and interpret these data in depth [16–19]. As prediction models based on radiomic features have shown promise in predicting tumor genotype, research interest in radiomics has been intensively studied [13, 20–24]. Previous studies have indicated that CT radiomic features can display spatial structure information in lesions that may be induced by EGFR mutations [25, 26]. Therefore, CT radiomic features can be used as a non-invasive and convenient method to predict EGFR mutations in patients with adenocarcinoma [25, 26]. Also, the EGFR signaling pathway plays an essential role in maintaining the aerobic glycolysis of tumor cells, and TKI can reverse the Warburg effect (tumor cells mainly rely on glycolysis to generate energy to maintain their rapid proliferation even in the presence of sufficient oxygen) of lung cancer cells [27, 28], which may lead to metabolic heterogeneity between tumor lesions with EGFR mutations and lesions with wild-type EGFR. Recently, although several reports have pointed out that the radiomic features of ^{18}F -Fluorodeoxyglucose (FDG) positron emission tomography/computed tomography (PET/CT) can reflect the metabolic heterogeneity of tumors and provide additional information for predicting EGFR gene status, there has been little research in this area [13, 20–24]. In addition, some clinical factors have been also considered to be risk factors for EGFR mutations, including females, never-smokers, and Asians with adenocarcinoma histology [29]. These clinical factors can provide guidance for TKI treatment to some extent when the results of molecular diagnosis are not available. For the above reasons, this study established four alternative models based on CT radiomic features, PET radiomic features, clinical factors, and PET/CT radiomic features combined with clinical factors, respectively, to find a prediction model that can make up for the deficiency of EGFR molecular detection by comparing each model's performance in predicting EGFR mutations of lung adenocarcinoma.

Patients and methods

Patient selection. This retrospective investigation followed the Declaration of Helsinki and was conducted with the approval of the First Affiliated Hospital of Harbin Medical University Institutional Ethics Committee, and the informed consent was waived because of the study's non-interventional nature. We retrospectively analyzed 120 lung cancer patients diagnosed and treated in our hospital from January 2014 to January 2019. Patients were selected according to the inclusion and exclusion criteria, resulting in a total of 88 patients included in this study. The inclusion criteria were as follows: 1) all patients were pathologically diagnosed as lung adenocarcinoma; 2) patients underwent ^{18}F -FDG PET/CT scanning and EGFR gene mutation detection before receiving antitumor therapy; 3) other malignant tumors or manifestations were absent; and 4) clinical data including sex, age, smoking history, tumor locations, carcinoembryonic

antigen (CEA) levels, and clinical stages were complete. The exclusion criteria were as follows: 1) the boundary between the primary lesion and surrounding tissue was unclear; 2) pure ground-glass pulmonary nodule without FDG uptake; and 3) the size of the primary tumor lesion was not enough for texture analysis (the LIFEx software only calculates the texture features of lesions with the number of voxels ≥ 64).

Then the 88 enrolled patients were divided into two independent cohorts: 65 patients diagnosed between January 2014 and December 2017 constituted the training cohorts, and 23 patients diagnosed between January 2018 and January 2019 constituted the validation cohorts.

EGFR gene mutation detection. Cancer tissue samples were obtained via surgery or puncture. Lung cancer tissues were fixed in 10% neutral formalin solution, embedded in paraffin, and sectioned. Samples DNA extraction and EGFR mutations detection were performed according to the reagent instructions. The kits were provided by Amoy Diagnostics Co., Ltd., China. The amplification refractory mutation system (ARMS) polymerase chain reaction (PCR) method was applied for EGFR gene mutation detection. All PCR analyses were performed on the Stratagene M \times 3000P Real-Time PCR system (Agilent Technologies). Seven EGFR mutation sites were detected, including exon 19 deletion mutations, L858R point mutations, T790M mutations, exon 20 insertion mutations, G719X mutations, S768I mutations, and L861Q mutations. If any mutation at the above sites was detected, the lesion was classified as EGFR mutation, whereas others as EGFR wild-type.

Patients imaging. All patients were required to fast for 6–8 hours, and the venous blood glucose levels were controlled to be less than 8.0 mmol/l before intravenous injection of 3.7–7.4 MBq/kg of ^{18}F -FDG. The ^{18}F -FDG isotope (radiochemical purity >95%) was manufactured by a medical cyclotron (HM-12, Sumitomo Heavy Industries Ltd., Japan). The PET/CT scanning was accomplished with a 16-slice Gemini GXL PET/CT scanner (Philips Medical System) at 60 ± 5 min ^{18}F -FDG injection. Prior to the PET acquisition, a low-dose CT scan (tube voltage: 120kV, tube current: 50 mAs, slice thickness: 5.0 mm, pitch: 1.0) was acquired for the purpose of attenuation correction. PET images were acquired with 1.5 min of acquisition time per bed position and a total of 6–7 PET bed positions. The scan range was from the head to the mid-thigh according to the agency standard clinical protocols. After automatic random-correction and automatic scattering-correction, the line of response (LOR) reconstruction algorithm was used to reconstruct the image without post-reconstruction filtering.

Extraction of PET and CT radiomic features. One radiologist with 4 years of experience in chest imaging diagnosis used the LIFEx software (version 6.00, <http://www.lifexsoft.org>) to semi-automatically segment the region of interest (ROI) on the patient PET images in the training set with a threshold of 40% maximum standard uptake value (SUVmax) [30], and then simultaneously extracted the radiomic features

of PET and CT. Another radiologist with 10 years of experience independently completed the same procedure to extract the radiomic features of PET and CT. For PET and CT images, the default value of software was used for spatial resampling (PET: 4.0 mm × 4.0 mm × 4.0 mm and CT: 1.171875 mm × 1.171875 mm × 5.0 mm), intensity discretization (PET: 64.0 bin and CT: 400.0 bin) and intensity rescaling bounds (PET: 0.0–20.0 and CT: –1000.0–3000.0 Hounsfield unit). Ninety-two radiomic features were extracted, including conventional PET/CT indices, histogram features, shape features, grey-level co-occurrence matrix (GLCM), neighborhood grey-level different matrix (NGLDM), grey-level run-length matrix (GLRLM), grey-level zone-length matrix (GLZLM) (the mathematic formulas can be found on the website: <http://www.lifexsoft.org>).

Model establishment. In order to eliminate subjective differences in ROI segmentation by inter-observer and ensure the repeatability of radiomic features, after z-score standardization of 45 CT radiomic features and 47 PET radiomic features extracted by the two experienced radiologists, inter-observer intraclass correlation efficiency (ICC) >0.75 was used to filter features with excellent repeatability. Therefore, these radiomic features with ICC ≤0.75 were eliminated, and 43 CT texture features and 47 PET texture features were preserved.

Then, a least absolute shrinkage and selection operator (LASSO) algorithm was applied to further filter 43 CT radiomic features to simplify the model and reduce the risk of overfitting. The complexity of the LASSO regression model is controlled by the parameter λ (the larger the value of λ , the more coefficients of features are compressed to zero and deleted). The optimal λ value of 0.103 was chosen according to 10-fold cross-validation. Six CT radiomic features with nonzero coefficients were selected, including SHAPE_Sphericity, GLRLM_Short-run emphasis (SRE), GLRLM_Short-run high grey-level emphasis (SRHGE), NGLDM_Coarseness, NGLDM_Busyness, GLZLM_Short-zone emphasis (SZE). According to the features weighted by the LASSO coefficients, the CT radiomic signature score (CT.radscore) was calculated by the following formula: $CT.radscore = -0.283 + 0.061 \times SHAPE_Sphericity - 0.361 \times GLRLM_SRE - 0.473 \times GLRLM_SRHGE + 0.186 \times NGLDM_Coarseness - 0.005 \times NGLDM_Busyness - 0.176 \times GLZLM_SZE$. Finally, the Logistic Regression (LR) model (model-1) was established using CT.radscore data.

In the same way, LASSO with 10-fold cross-validation was applied to further filter 47 PET radiomic features. The optimal λ value was calculated to be 0.080. Six PET radiomic features with nonzero coefficients were obtained, including minimum standard uptake value (SUVmin), SHAPE_Sphericity, SHAPE_Compacity, GLCM_Energy, GLCM_Correlation, and GLZLM_Long-zone low grey-level emphasis (LZLGE). The PET radiomic signature score (PET.radscore) was calculated according to the following formula: $PET.radscore = -0.341 - 0.711 \times SUVmin + 0.137$

$\times SHAPE_Sphericity + 0.212 \times SHAPE_Compacity - 0.222 \times GLCM_Energy - 0.477 \times GLCM_Correlation - 0.077 \times GLZLM_LZLGE$. The LR model (model-2) was established using PET.radscore data.

The clinical data including sex, age, smoking history, tumor locations, CEA levels, and clinical stages were analyzed. Categorical variables were compared using the χ^2 test or Fisher's exact test, and continuous variables were analyzed by the independent samples t-test. All clinical factors were analyzed. Significant differences were observed in the distribution of sex ($p=0.004$) and smoking history ($p<0.001$) between the EGFR mutations group and the wild-type group; i.e., the EGFR mutations were more common in females and patients with no smoking history, whereas the EGFR wild-type was opposite, which has a higher incidence in males and patients with a history of smoking. Therefore, these clinical factors that are significantly different from EGFR mutations and wild-type were put into the LR model to establish model-3. Model-4 was established by CT.radscore, PET.radscore, and clinical factors.

Receiver operating characteristic (ROC) curve analysis was employed to evaluate the performance of the model in the training set. The DeLong test was used to compare the discrimination performance of all constructed models to select the best model. Subsequently, we drew a nomogram of the optimal model to show the predictive effect more intuitively.

Model validation and evaluation. A radiologist with 3 years of experience in chest imaging diagnosis processed image data of patients in the validation set, and extracted PET and CT radiomic features using the LIFEx software. Next, the nomogram was used to predict the validation set data. The concordance index (C-index) value, sensitivity, specificity, and accuracy were used to evaluate the prediction performance of the nomogram model. The calibration curves and Hosmer-Lemeshow test was used to evaluate the calibration of the nomogram model. In addition, the decision curve analysis (DCA) was used to assess the net benefit of the nomogram.

Statistical analysis. Data analysis was performed using SPSS software version 25.0 (SPSS, Chicago, IL, USA) and R language (version 3.6.3). The R package "glmnet" was used to perform LASSO regression and LR model; the R package "pROC" was used for ROC analysis; the R package "rms" was used to perform nomogram model; the R package "riskRegression" was used to draw calibration curve, and the R package "ResourceSelection" was used to perform the Hosmer-Lemeshow test. DCA curve was performed using "rmda" package. A p-value <0.05 was considered statistically significant.

Results

Patient characteristics. In this study, 88 patients with lung adenocarcinoma were registered, and their clinical data such

Table 1. Patient characteristics.

Characteristics	Training		p-value	Validation		p-value
	Mutant EGFR	Wild-type EGFR		Mutant EGFR	Wild-type EGFR	
Sex			0.004			0.018
Male	8 (28.6%)	24 (64.9%)		4 (44.4%)	13 (92.9%)	
Female	20 (71.4%)	13 (35.1%)		5 (55.6%)	1 (7.1%)	
Age (mean±SD)	61.29±11.77	61.46±11.58	0.953	68.44±10.58	65.71±13.05	0.605
Smoking history			<0.001			0.077
Smoker	1 (3.6%)	16 (43.2%)		3 (33.3%)	11 (78.6%)	
Never	27 (96.4%)	21 (56.8%)		6 (66.7%)	3 (21.4%)	
Location			0.605			0.120
Right upper lobe	7 (25.0%)	10 (27.8%)		2 (22.2%)	6 (42.9%)	
Right middle lobe	1 (3.6%)	5 (13.9%)		1 (11.1%)	0 (0.0%)	
Right lower lobe	8 (28.6%)	11 (30.6%)		2 (22.2%)	6 (42.9%)	
Left upper lobe	7 (25.0%)	5 (13.9%)		4 (44.4%)	1 (7.1%)	
Left lower lobe	3 (10.7%)	6 (16.2%)		0 (0.0%)	1 (7.1%)	
Overlapping lesion	2 (7.1%)	0 (0.0%)		0 (0.0%)	0 (0.0%)	
CEA level			0.362			0.102
≥5.0 ng/ml	19 (67.9%)	21 (56.8%)		3 (33.3%)	10 (71.4%)	
<5.0 ng/ml	9 (32.1%)	16 (43.2%)		6 (66.7%)	4 (28.6%)	
Stage			0.271			0.657
I–II	5 (17.9%)	11 (29.7%)		5 (55.6%)	10 (71.4%)	
III–IV	23 (82.1%)	26 (70.3%)		4 (44.4%)	4 (28.6%)	

EGFR, epidermal growth factor receptor; SD, standard deviation; CEA, carcinoembryonic antigen

Table 2. DeLong test within different models.

Prediction model-A	Prediction model-B	p-value
model-4	model-1	0.021
model-4	model-2	0.013
model-4	model-3	0.049
model-1	model-2	0.895
model-1	model-3	0.458
model-2	model-3	0.476

as sex, age, smoking history, tumor locations, CEA levels, and clinical stages were analyzed. The complete characteristics of the training cohort and validation cohort are described in Table 1.

Performance of the models. In this study, we constructed four models in the training cohort based on different factors. The AUC values ranged from 0.715 to 0.864 in four models (orders 1–4). All the prediction models showed a good predictive performance. The ROC curves and parameters of all the models in the training group are presented in Figures 1A–1D.

In terms of area under the curve, model-4 showed relatively high accuracy (AUC = 0.864), model-3 was slightly better than model-1 and model-2, and model-1 had the lowest accuracy (AUC = 0.715). The DeLong test was used for pairwise comparison of four prediction models to assess whether the difference in AUC between the prediction

models was statistically significant. Significant differences were observed in the AUC between model-4 and the other three (model-4 vs. model-1: $p=0.021$; model-4 vs. model-2: $p=0.013$; model-4 vs. model-3: $p=0.049$). Comparing model-1, model-2, and model-3 in pairs, the DeLong test revealed that the AUC values of the three prediction models were not significantly different. The comparison results of each prediction model are summarized in Table 2.

Validation of nomogram and evaluation of clinical utility. Considering that model-4, which combined radiomic features with clinical factors demonstrates the best predictive ability, we established a nomogram of model-4 to facilitate the visualization of the nomogram results of the prediction outcome and the proportion of each factor, as shown in Figure 2. The nomogram was used to predict 23 patients in the validation set, and the C-index value was 0.778 (95%CI: 0.585–0.970), with a sensitivity of 0.556, a specificity of 0.857, and an accuracy of 0.739, indicating that the model has moderate discriminability and prediction accuracy. The model calibration curve is shown in Figure 3. The Hosmer-Lemeshow test can reflect the difference between the model predicted value and the actual value, and the result showed that the difference was not statistically significant ($\chi^2=6.685$, $p=0.154$), which proved that the model had a good calibration. Moreover, we used the DCA curve to verify the net benefit of the nomogram model in predicting the EGFR mutations and observed that the nomogram model is beneficial for patients with a wide range of risk thresholds. The DCA curves of the nomogram are displayed in Figure 4.

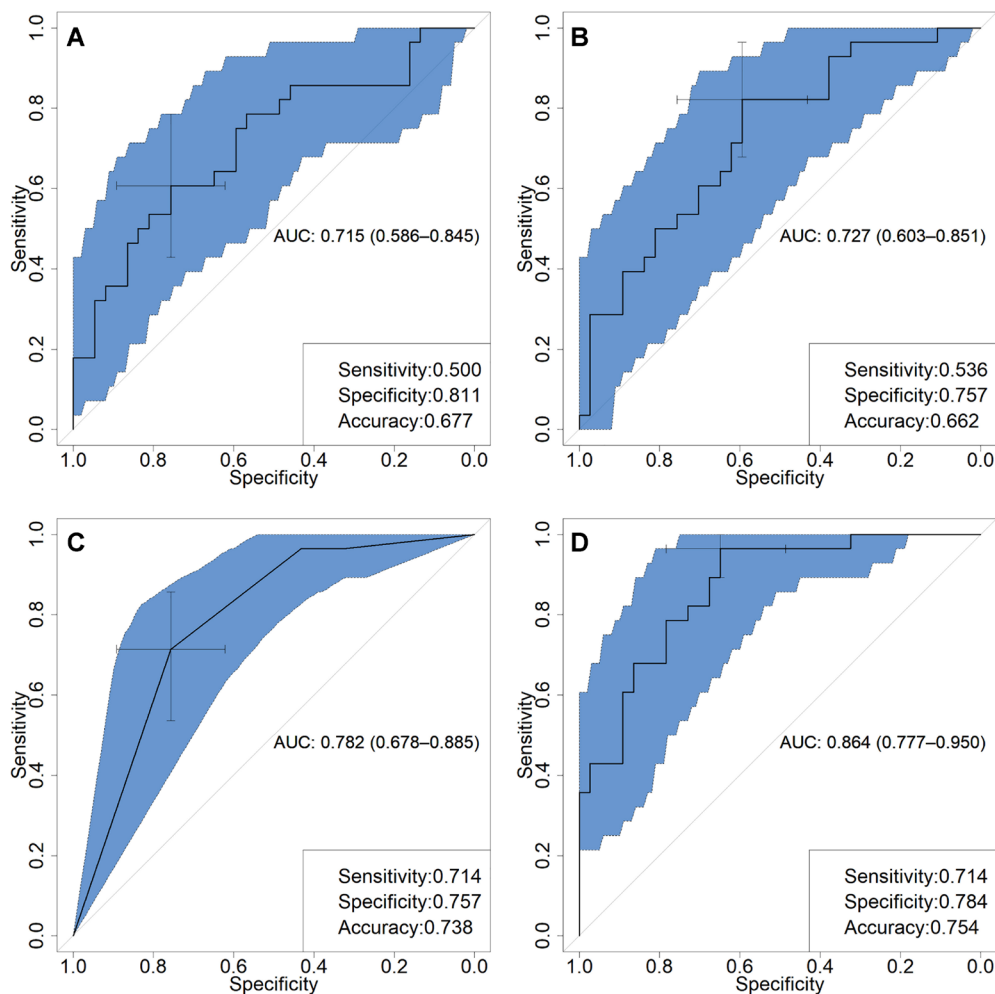


Figure 1. The ROC curves of the prediction models. The blue area represents the 95% confidence interval, and the cross-marked point represents the best threshold point. A–D) Represent model-1, model-2, model-3, and model-4, respectively. Abbreviations: ROC-receiver operating characteristic

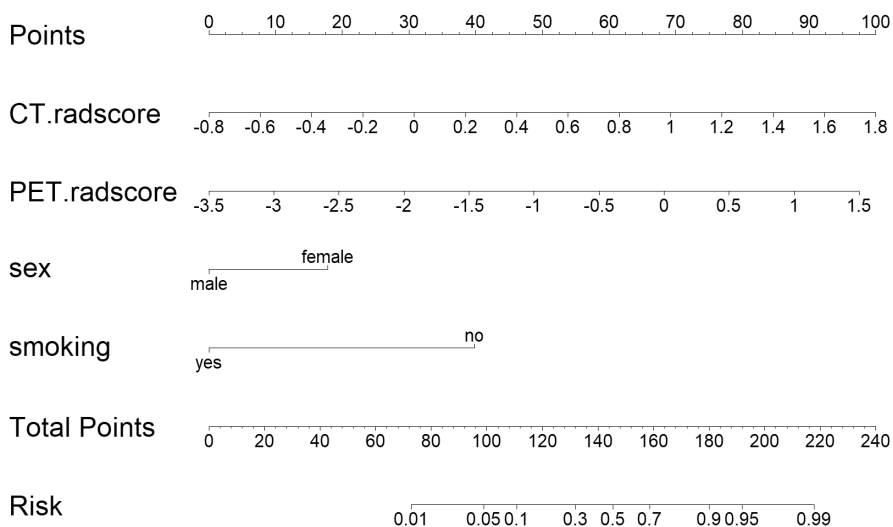


Figure 2. Nomogram model for predicting EGFR mutations. EGFR: epidermal growth factor receptor.

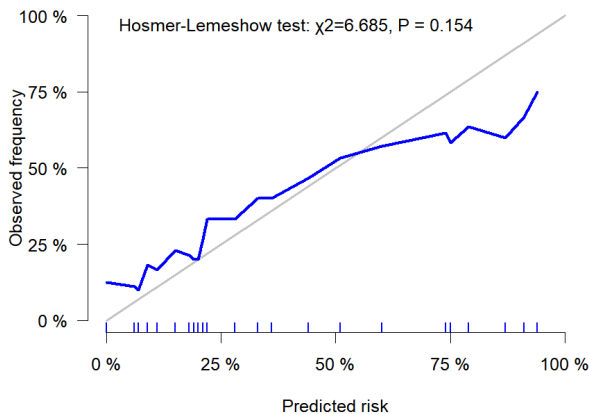


Figure 3. Calibration curves of the nomogram model in the validation set. The y-axis represents the actual incidence of EGFR mutations. The x-axis represents the predicted probability of the EGFR mutations. The solid diagonal gray line represents the ideal model, which means the predicted probability is completely consistent with the actual incidence and the solid blue line represents the nomogram model calibration curve. Abbreviations: EGFR-epidermal growth factor receptor

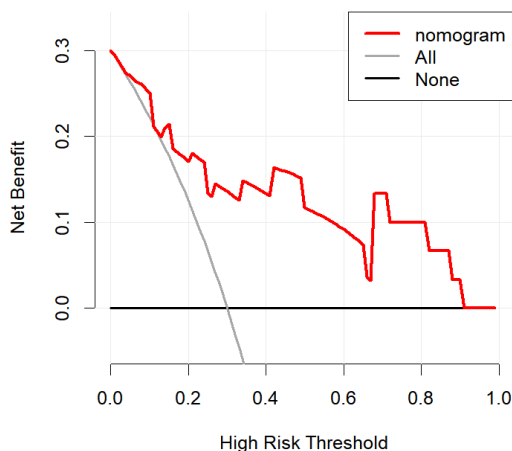


Figure 4. DCA curve of nomogram model in the validation set. The Y-axis and the X-axis represent the net benefit and risk threshold respectively. The red line indicates the nomogram model, the grey oblique line indicates the hypothesis that all patients were with EGFR mutations, the horizontal black line represents the hypothesis that all patients were EGFR wild-type. Abbreviations: DCA-decision curve analysis; EGFR-epidermal growth factor receptor

Discussion

It is well known that the assessment of the EGFR gene mutation status is conducive for selecting favorable therapeutic schemes and predicting the efficacy of EGFR-TKI in patients with lung adenocarcinoma [31, 32]. However, the heterogeneity and the aggressiveness of molecular diagnosis may influence the assessment of EGFR mutations [12, 13]. Although EGFR gene mutation status can be aided by liquid biopsy in clinical practice, when the tumor is small, there may not be enough DNA in the liquid to reduce the accuracy

of the test [33]. Radiogenomics is a branch of radiomics, whose purpose is concerned with the relationship between quantitative texture features and genomics [34, 35]. With the increasing evidence of the correlation between texture features and EGFR gene status in lung cancer patients, radiomics based on ^{18}F -FDG PET/CT is expected to play an important supplemental role in the precision treatment of lung cancer [13, 20–24].

The backbone of radiomics is the development of clinical models to predict patient outcomes, thereby facilitating better clinical management of patients. In previous reports, most researchers used CT texture features to establish EGFR mutations prediction models, but the evidence for predicting EGFR mutations using PET radiomic features was insufficient [13, 20–24]. Yip et al. first explored the value of ^{18}F -FDG PET radiomic features in predicting EGFR mutations in non-small cell lung cancer (NSCLC) and found that PET radiomic features can reflect the differences in tumor metabolic phenotypes caused by EGFR mutations [20]. The results of our study further confirmed this point of view. The AUC value of model-2 established by PET radiomic features in the experiment was 0.727. However, in terms of the results, the model using PET radiomic features alone is not very satisfactory. In another report, Koyasu et al. analyzed the PET/CT images of 138 non-small cell lung patients from public databases. They used Bayesian optimization to select the optimal combination of seven PET and CT radiomic features and then established an eXtreme Gradient Boosting (XGB) model to predict EGFR mutations, with an AUC of 0.659 [24]. The study by Nair et al. was similar to the report of Koyasu et al. PET and CT radiomic features were used in the study of Nair et al. to establish a complex LR model capable of distinguishing EGFR mutant and wild-type, with an AUC of 0.870, a sensitivity of 0.760, a specificity of 0.660, and an accuracy of 0.710 [22]. Additionally, Jiang et al. retrospectively analyzed 80 patients with non-small cell lung cancer, and the results showed that combining semantic characteristics in PET/CT texture features could improve the effect of the model in predicting EGFR mutations, with an increase of AUC value by 12% [21]. However, whether the difference is statistically significant has not been further tested. Another problem is that although semantic characteristics are more accessible in clinical practice, they are more influenced by observers.

Compared with previous studies, a major advantage of our study is that clinical information such as sex and smoking history was introduced into the model. These clinical factors that can be obtained through medical history are more objective and appear to avoid the instability caused by semantic characteristics. Moreover, there is considerable evidence that these clinical factors contribute to the prediction of EGFR mutations [29]. To confirm the value of clinical factors, we used clinical factors to construct model-3 in our study. In the data of the training set, the AUC value of model-3 was 0.782, which was slightly better than the prediction performance of the model established by using PET radiomic features

alone or CT radiomic features alone. Furthermore, when comparing the models, it was found that model-1 based on CT radiomic features had the worst effect. In our analysis, the reason for this result might be that the ROI segmentation was based on PET images, which might have an impact on the value of CT radiomic features in the process of feature extraction from matching CT images.

Our results showed that model-4 established by combining PET/CT texture features with clinical factors is superior to the other models in the prediction of EGFR mutations, and the difference between model-4 and the other models is statistically significant. This result is consistent with the two previous studies [13, 23]. Li et al. analyzed the PET/CT radiomic features of 115 patients with non-small cell lung cancer. The AUC value increased from 0.805 to 0.822 after adding clinical factors to the model [13]. Zhang et al. established the LR model using PET/CT radiomic features of 248 patients with lung adenocarcinoma, and then combined clinical factors to establish a new model. The prediction performance of the new model was better than that of the model based only on radiomic features [23]. Besides, according to the PET/CT radiomic features and two clinical risk factors (sex and smoking), we created a nomogram that can visually predict the risk of EGFR mutations. Subsequently, we further evaluated the nomogram in a validation cohort of 23 patients with lung adenocarcinoma. The C-index value of the model was 0.778 (95% CI: 0.585–0.970), with an accuracy of 0.739, indicating that the model had moderate discriminability and prediction accuracy. And the results of the calibration curve and Hosmer-Lemeshow test showed that the predicted result of the model accorded well with the actual situation, which proved that the model had a good calibration. Since the AUC value only focuses on the accuracy of the model's prediction [36], the DCA curve, by comprehensively weighing the pros and cons of the prediction model, also measures the clinical utility of a model [37]. Thus, the DCA curves of prediction models were drawn. Based on the obtained results, the nomogram we established has good clinical utility. It is very important to note that clinical factors and radiomic features are complementary rather than antithetical, which can provide different information for the detection of EGFR mutations in lung adenocarcinoma cancer. Introducing different factors into the established model can provide a more accurate model for clinical practice.

There were some limitations of this study. Firstly, our model was based on a single-central sample and lack of an independent cohort for external validation of the stability of the model, which affects the generalization ability of the model to a certain extent. Secondly, due to our small sample size, the prediction models were established by the LR model, which is often used in small sample size because of its ability to their resistivity to overfitting. It is doubtless that the use of a large sample size is conducive to the construction of a more accurate prediction model. Thirdly, due to the limitation of the reconstruction technique, the image blurs caused

by respiratory motion may affect the quantification of PET radiomic features. The effect of respiratory movement on the texture features of lung tumors varies with the location of the lesions. For instance, the effect is the least in the upper lobe and more significant in the lower lobe [17]. However, a previous report indicated that although the presence or absence of respiratory gating affects the value of texture features, this effect does not interfere with the prognostic value of texture features [38]. As far as we are concerned, eliminating as many interference factors as possible is beneficial for the development of an accurate model. In a report by Orhac et al., we note that the ComBat method, originally developed for addressing the problem of a batch effect in genomics, can coordinate the influence of different acquisition and reconstruction conditions on texture features [39]. Finally, in the process of tumor lesion segmentation, ROI was obtained from PET images. When the same ROI was applied to CT images, some external tumor tissues might be segmented along with the tumor, which may adversely affect the predictive effect of the model.

In summary, the EGFR prediction model established by ¹⁸F-FDG PET/CT radiomic features in combination with clinical factors could identify the EGFR mutations. The model we established had good discriminability, prediction accuracy, calibration, and net benefit. The result showed that ¹⁸F-FDG PET/CT radiomics was expected to become an important supplement to gene detection and provide a new biomarker for guiding TKI-targeted therapy in patients with lung adenocarcinoma. It is worth noting that some recent reports on dynamic changes of texture features and ¹⁸F-fluorothymidine(FLT)-PET texture features provide some new ideas for the study of radiomics [40, 41]. Of course, a large sample size and multi-center study can accelerate the early realization of clinical application of models based on radiomic features.

Acknowledgments: The authors thank the patients and their families for participation in the study and Lintian Jiang for English writing assistance.

References

- [1] LIN LI, XU CW, ZHANG BO, LIU RR, GE FJ et al. Clinicopathological observation of primary lung enteric adenocarcinoma and its response to chemotherapy: A case report and review of the literature. *Exp Ther Med* 2016; 11: 201–207. <https://doi.org/10.3892/etm.2015.2864>
- [2] WANG L, LI X, REN Y, GENG H, ZHANG Q et al. Cancer-associated fibroblasts contribute to cisplatin resistance by modulating ANXA3 in lung cancer cells. *Cancer Sci* 2019; 110: 1609–1620. <https://doi.org/10.1111/cas.13998>
- [3] ZHANG M, JIANG N, CUI R, DU S, OU H et al. Deregulated lncRNA expression profile in the mouse lung adenocarcinomas with KRAS-G12D mutation and P53 knockout. *J Cell Mol Med* 2019; 23: 6978–6988. <https://doi.org/10.1111/jcmm.14584>

- [4] FANG P, ZHANG L, ZHANG X, YU J, SUN J et al. Apatinib Mesylate in the treatment of advanced progressed lung adenocarcinoma patients with EGFR-TKI resistance -A Multi-center Randomized Trial. *Sci Rep* 2019; 9: 14013. <https://doi.org/10.1038/s41598-019-50350-6>
- [5] BOUSQUET MUR E, BERNARDO S, PAPON L, MANCINI M, FABBRIZIO E et al. Notch inhibition overcomes resistance to tyrosine kinase inhibitors in EGFR-driven lung adenocarcinoma. *J Clin Invest* 2020; 130: 612–624. <https://doi.org/10.1172/JCI126896>
- [6] YU S, LIU D, SHEN B, SHI M, FENG J. Immunotherapy strategy of EGFR mutant lung cancer. *Am J Cancer Res* 2018; 8: 2106–2115.
- [7] LI K, YANG M, LIANG N, LI S. Determining EGFR-TKI sensitivity of G719X and other uncommon EGFR mutations in non-small cell lung cancer: Perplexity and solution (Review). *Oncol Rep* 2017; 37: 1347–1358. <https://doi.org/10.3892/or.2017.5409>
- [8] OKAMOTO I, MORITA S, TASHIRO N, IMAMURA F, INOUE A et al. Real world treatment and outcomes in EGFR mutation-positive non-small cell lung cancer: Long-term follow-up of a large patient cohort. *Lung Cancer* 2018; 117: 14–19. <https://doi.org/10.1016/j.lungcan.2018.01.005>
- [9] ABDURAHMAN A, ANWAR J, TURGHUN A, NIYAZ M, ZHANG L et al. Epidermal growth factor receptor gene mutation status and its association with clinical characteristics and tumor markers in non-small-cell lung cancer patients in Northwest China. *Mol Clin Oncol* 2015; 3: 847–850. <https://doi.org/10.3892/mco.2015.564>
- [10] WU YL, ZHOU C, HU CP, FENG J, LU S et al. Afatinib versus cisplatin plus gemcitabine for first-line treatment of Asian patients with advanced non-small-cell lung cancer harbouring EGFR mutations (LUX-Lung 6): an open-label, randomised phase 3 trial. *Lancet Oncol* 2014; 15: 213–222. [https://doi.org/10.1016/S1470-2045\(13\)70604-1](https://doi.org/10.1016/S1470-2045(13)70604-1)
- [11] REN Y, YAO Y, MA Q, ZHONG D. EGFR gene-mutation status correlated with therapeutic decision making in lung adenocarcinoma. *Onco Targets Ther* 2015; 8: 3017–3020. <https://doi.org/10.2147/OTT.S87146>
- [12] NIU L, SONG X, WANG N, XUE L, SONG X et al. Tumor-derived exosomal proteins as diagnostic biomarkers in non-small cell lung cancer. *Cancer Sci* 2019; 110: 433–442. <https://doi.org/10.1111/cas.13862>
- [13] LI X, YIN G, ZHANG Y, DAI D, LIU J et al. Predictive Power of a Radiomic Signature Based on 18F-FDG PET/CT Images for EGFR Mutational Status in NSCLC. *Front Oncol* 2019; 9: 1062. <https://doi.org/10.3389/fonc.2019.01062>
- [14] WEI B, ZHAO C, LI J, ZHAO J, REN P et al. Combined plasma and tissue genotyping of EGFR T790M benefits NSCLC patients: a real-world clinical example. *Mol Oncol* 2019; 13: 1226–1234. <https://doi.org/10.1002/1878-0261.12481>
- [15] LV P, YANG S, LIU W, QIN H, TANG X et al. Circulating plasma lncRNAs as novel markers of EGFR mutation status and monitors of epidermal growth factor receptor-tyrosine kinase inhibitor therapy. *Thorac Cancer* 2020; 11: 29–40. <https://doi.org/10.1111/1759-7714.13216>
- [16] KONG Z, LIN Y, JIANG C, LI L, LIU Z et al. 18F-FDG-PET-based Radiomics signature predicts MGMT promoter methylation status in primary diffuse glioma. *Cancer Imaging* 2019; 19: 58. <https://doi.org/10.1186/s40644-019-0246-0>
- [17] HA S, CHOI H, PAENG JC, CHEON GJ. Radiomics in Oncological PET/CT: a Methodological Overview. *Nucl Med Mol Imaging* 2019; 53: 14–29. <https://doi.org/10.1007/s13139-019-00571-4>
- [18] WU J, THA KK, XING L, LI R. Radiomics and radiogenomics for precision radiotherapy. *J Radiat Res* 2018; 59: i25–i31. <https://doi.org/10.1093/jrr/rrx102>
- [19] LAMBIN P, LEIJENAAR RTH, DEIST TM, PEERLINGS J, DE JONG EEC et al. Radiomics: the bridge between medical imaging and personalized medicine. *Nat Rev Clin Oncol* 2017; 14: 749–762. <https://doi.org/10.1038/nrcli-nonc.2017.141>
- [20] YIP SS, KIM J, COROLLER TP, PARMAR C, VELAZQUEZ ER et al. Associations Between Somatic Mutations and Metabolic Imaging Phenotypes in Non-Small Cell Lung Cancer. *J Nucl Med* 2017; 58: 569–576. <https://doi.org/10.2967/jnumed.116.181826>
- [21] JIANG M, ZHANG Y, XU J, JI M, GUO Y et al. Assessing EGFR gene mutation status in non-small cell lung cancer with imaging features from PET/CT. *Nucl Med Commun* 2019; 40: 842–849. <https://doi.org/10.1097/MNM.0000000000001043>
- [22] NAIR JKR, SAEED UA, MCDUGALL CC, SABRI A, KOVACINA B et al. Radiogenomic Models Using Machine Learning Techniques to Predict EGFR Mutations in Non-Small Cell Lung Cancer. *Can Assoc Radiol J* 2020; 846537119899526. <https://doi.org/10.1177/0846537119899526>
- [23] ZHANG J, ZHAO X, ZHAO Y, ZHANG J, ZHANG Z et al. Value of pre-therapy 18F-FDG PET/CT radiomics in predicting EGFR mutation status in patients with non-small cell lung cancer. *Eur J Nucl Med Mol Imaging* 2020; 47: 1137–1146. <https://doi.org/10.1007/s00259-019-04592-1>
- [24] KOYASU S, NISHIO M, ISODA H, NAKAMOTO Y, TOGASHI K. Usefulness of gradient tree boosting for predicting histological subtype and EGFR mutation status of non-small cell lung cancer on 18F FDG-PET/CT. *Ann Nucl Med* 2020; 34: 49–57. <https://doi.org/10.1007/s12149-019-01414-0>
- [25] WANG X, KONG C, XU W, YANG S, SHI D et al. Decoding tumor mutation burden and driver mutations in early stage lung adenocarcinoma using CT-based radiomics signature. *Thorac Cancer* 2019; 10: 1904–1912. <https://doi.org/10.1111/1759-7714.13163>
- [26] LIU Y, KIM J, BALAGURUNATHAN Y, LI Q, GARCIA AL et al. Radiomic Features Are Associated With EGFR Mutation Status in Lung Adenocarcinomas. *Clin Lung Cancer* 2016; 17: 441–448.e6. <https://doi.org/10.1016/j.clc.2016.02.001>
- [27] MAKINOSHIMA H, TAKITA M, MATSUMOTO S, YAGISHITA A, OWADA S et al. Epidermal growth factor receptor (EGFR) signaling regulates global metabolic pathways in EGFR-mutated lung adenocarcinoma. *J Biol Chem* 2014; 289: 20813–20823. <https://doi.org/10.1074/jbc.M114.575464>

- [28] DE ROSA V, IOMMELLI F, MONTI M, FONTI R, VOTTA G et al. Reversal of Warburg effect and reactivation of oxidative Phosphorylation by differential inhibition of EGFR signaling pathways in non-small cell lung cancer. *Clin Cancer Res* 2015; 21: 5110–5120. <https://doi.org/10.1158/1078-0432.CCR-15-0375>
- [29] SASAKI H, SHITARA M, YOKOTA K, OKUDA K, HIKOSAKA Y et al. Braf and erbB2 mutations correlate with smoking status in lung cancer patients. *Exp Ther Med* 2012; 3: 771–775. <https://doi.org/10.3892/etm.2012.500>
- [30] NIOCHE C, ORLHAC F, BOUGHDAD S, REUZÉ S, GOYA-OUTI J et al. LIFEx: A Freeware for Radiomic Feature Calculation in Multimodality Imaging to Accelerate Advances in the Characterization of Tumor Heterogeneity. *Cancer Res* 2018; 78: 4786–4789. <https://doi.org/10.1158/0008-5472.CAN-18-0125>
- [31] ZHOU X, CAI L, LIU J, HUA X, ZHANG Y et al. Analyzing EGFR mutations and their association with clinicopathological characteristics and prognosis of patients with lung adenocarcinoma. *Oncol Lett* 2018; 16: 362–370. <https://doi.org/10.3892/ol.2018.8681>
- [32] LV P, YANG S, LIU W, QIN H, TANG X et al. Circulating plasma lncRNAs as novel markers of EGFR mutation status and monitors of epidermal growth factor receptor-tyrosine kinase inhibitor therapy. *Thorac Cancer* 2020; 11: 29–40. <https://doi.org/10.1111/1759-7714.13216>
- [33] SORIA-COMES T, PALOMAR-ABRIL V, URESTE MM, GUEROLA MT, MAIQUES ICM. Real-World Data of the Correlation between EGFR Determination by Liquid Biopsy in Non-squamous Non-small Cell Lung Cancer (NSCLC) and the EGFR Profile in Tumor Biopsy. *Pathol Oncol Res* 2020; 26: 845–851. <https://doi.org/10.1007/s12253-019-00628-x>
- [34] LAMBIN P, RIOS-VELAZQUEZ E, LEIJENAAR R, CARVALHO S, VAN STIPHOUT RG et al. Radiomics: extracting more information from medical images using advanced feature analysis. *Eur J Cancer* 2012; 48: 441–446. <https://doi.org/10.1016/j.ejca.2011.11.036>
- [35] OU J, LI R, ZENG R, WU CQ, CHEN Y et al. CT radiomic features for predicting resectability of oesophageal squamous cell carcinoma as given by feature analysis: a case control study. *Cancer Imaging* 2019; 19: 66. <https://doi.org/10.1186/s40644-019-0254-0>
- [36] LI Y, GE D, GU J, XU F, ZHU Q et al. A large cohort study identifying a novel prognosis prediction model for lung adenocarcinoma through machine learning strategies. *BMC Cancer* 2019; 19: 886. <https://doi.org/10.1186/s12885-019-6101-7>
- [37] LI X, YU W, LIANG C, XU Y, ZHANG M et al. INHBA is a prognostic predictor for patients with colon adenocarcinoma. *BMC Cancer* 2020; 20: 305. <https://doi.org/10.1186/s12885-020-06743-2>
- [38] GROOTJANS W, TIXIER F, VAN DER VOS CS, VRIENS D, LE REST CC et al. The impact of optimal respiratory gating and image noise on evaluation of intratumor heterogeneity on 18F-FDG PET imaging of lung cancer. *J Nucl Med* 2016; 57: 1692–1698. <https://doi.org/10.2967/jnumed.116.173112>
- [39] ORLHAC F, BOUGHDAD S, PHILIPPE C, STALLA-BOURDILLON H, NIOCHE C et al. A postreconstruction harmonization method for multicenter radiomic studies in PET. *J Nucl Med* 2018; 59: 1321–1328. <https://doi.org/10.2967/jnumed.117.199935>
- [40] CHENG L, ZHANG J, WANG Y, XU X, ZHANG Y et al. Textural features of 18F-FDG PET after two cycles of neoadjuvant chemotherapy can predict pCR in patients with locally advanced breast cancer. *Ann Nucl Med* 2017; 31: 544–552. <https://doi.org/10.1007/s12149-017-1184-1>
- [41] ULRICH EJ, MENDA Y, BOLES PONTO LL, ANDERSON CM, SMITH BJ et al. FLT PET Radiomics for Response Prediction to Chemoradiation Therapy in Head and Neck Squamous Cell Cancer. *Tomography* 2019; 5: 161–169. <https://doi.org/10.18383/j.tom.2018.00038>